Supporting Information

Isomorphic BODIPY-based metal-organic frameworks for high-efficiency photoredox organic transformations

Chen-Yang Nie, [a] Li-Jun Xue, [a] Shao-Dan Wang, [a] Meng-Yuan Li, [a] Qian Kang [a] and Li-Li Wen* [a]

[a] Engineering Research Center of Photoenergy Utilization for Pollution Control and Carbon Reduction, Ministry of Education; College of Chemistry, Central China Normal University, Wuhan 430079, P. R. China.

*Corresponding Author. E-mail: wenlili@ccnu.edu.cn (L. L. Wen)

Materials and Instruments

The Fourier transform infrared (FT-IR) spectra were collected in the range of 4000-400 cm^{-1} on a Bruker Tensor 27 spectrometer with KBr pellets dispersed samples. The powder X-ray diffraction (PXRD) pattern on the samples were recorded on Cu Kα radiation (λ = 1.5406 Å) over a 2θ range of 5-40°. The UV/Vis diffused reflectance spectra (DRS) were obtained on Agilent Cary 100 spectrophotometer with $BaSO_4$ as the reference for the baseline correction. Room temperature steady-state photoluminescence (PL) and time-resolved photoluminescence (TRPL) of the samples were collected on a FLS1000 fluorescence spectrophotometer. Electron paramagnetic resonance (EPR) spectra was measured by a Bruker EMXmicro EPR. Scanning frequency: 9.83 GHz; central field: 3508.25 G; scanning power: 0.2 mW; scanning temperature: 25 °C. The starting materials were commercially available and were used without further purification. After the catalytic reaction, the product was performed on a Gas chromatograph (GC) with a flame ionization detector (FID).

Experimental Section

X-ray Crystallography. All crystallographic data were recorded at a Bruker D8 Venture area-detector diffractometer with Ga-Kα radiation at 100 K. The structures were solved by the direct methods and refined by full-matrix least-squares refinements based on F^2 using the SHELXTL crystallographic software package.[1,2] In the structure, free solvent molecules were removed using the SQUEEZE routine of PLATON,[3] All the non-hydrogen atoms were refined anisotropically. The positions of hydrogen atoms on carbon atoms were calculated theoretically. Parameters of the crystal data collection and refinement are given in Table S1. The Cambridge Crystallographic Data Centre (CCDC) number is 2296424 and 2323638. Select bond lengths and angles are provided in Table S2 and Table S3.

Electrochemical measurements. Photoelectrochemical measurements were performed on an electrochemical workstation (CHI760e Instruments). The preparation method of the working electrode is as follows: First, weigh 10 mg of compounds **1** and **2** and put it into the quartz glass vial, adding 1.0 mL mixed solution of ethanol and distilled water (v/v=1) and 20 μl Nafion mixture solution, subsequently, ultrasound for 30 minutes. Then, 100 μl mixture was transferred into the FTO with 1 × 1 cm^2 illuminated area and dried at room temperature. Platinum electrode as the auxiliary electrode, Ag/AgCl electrode as reference electrode, Na_2SO_4 (0.5 M) solution was used as the electrolyte solution. Mott−Schottky (M−S) plots were recorded in the dark at frequencies of 1000 Hz, 1500 Hz and 2000 Hz. The on−off transient photocurrent responses were recorded with a sampling interval of 25 s using a 300 W Xe lamp with full spectrum. Electrochemical impedance spectroscopy measurements were recorded over a 0.01 to 10^6 Hz frequency range.

Scavenger Experiments. A series of photocatalyst-free radical scavengers were used to control the photoactivity experiments, i.e., KI and $AgNO_3$ were employed as the scavenger of photogenerated holes and electrons, t-butanol as the scavenger of hydroxyl radicals (•OH), 2,2,6,6-tetramethylpiperidinyl-1-oxide (TEMPO) as the scavenger of α-carbonyl radical, 1,4-benzoquinone (BQ) as the scavenger of superoxide radical species ($O_2^{\bullet-}$), and 1,4-diazabicyclo[2.2.2]octane (DABCO) as the scavenger of singlet oxygen ($^1O_2$).

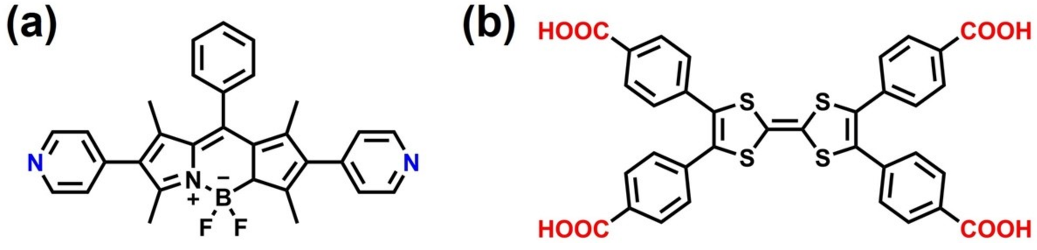

Scheme S1. The structure of BODIPY (a) and H_4TTFTB(b)

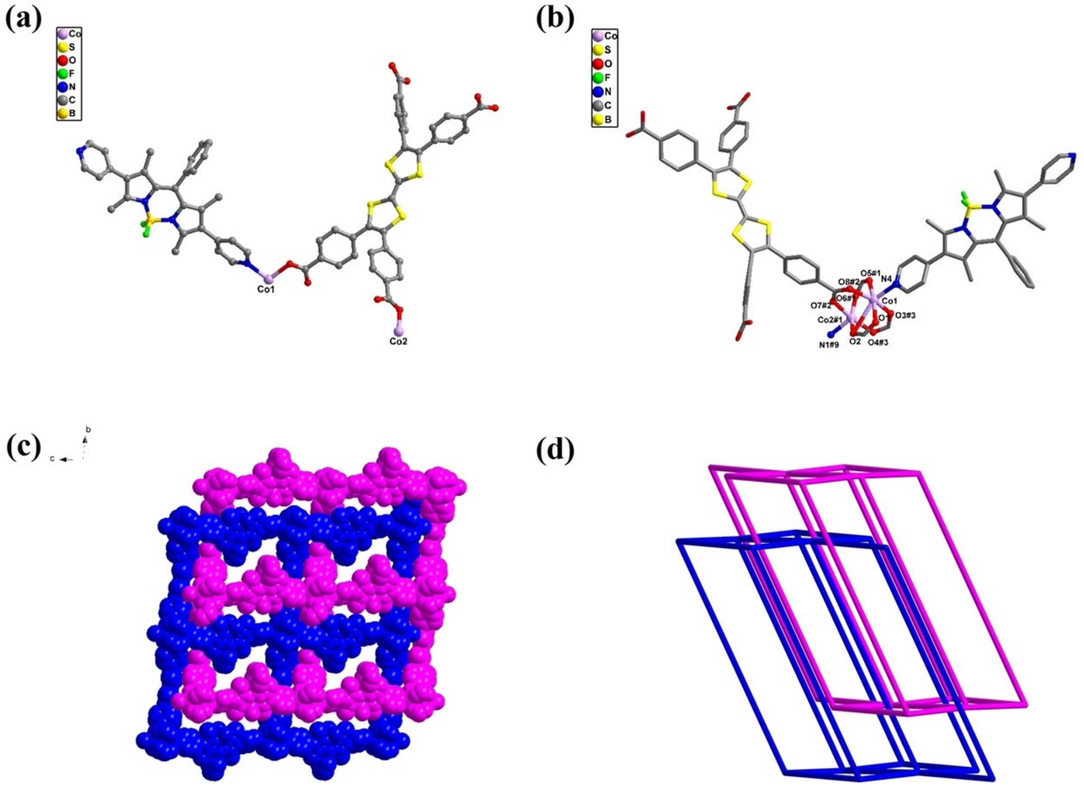

Fig. S1. Compound **2**: (a) The asymmetric unit; (b) Coordination environments of the Co^{II} ion (H atoms are omitted for clarity); (c) space-filling mode of **2**; (d) Schematic of the 2-fold interpenetration. The symmetry codes refer to Table S3.

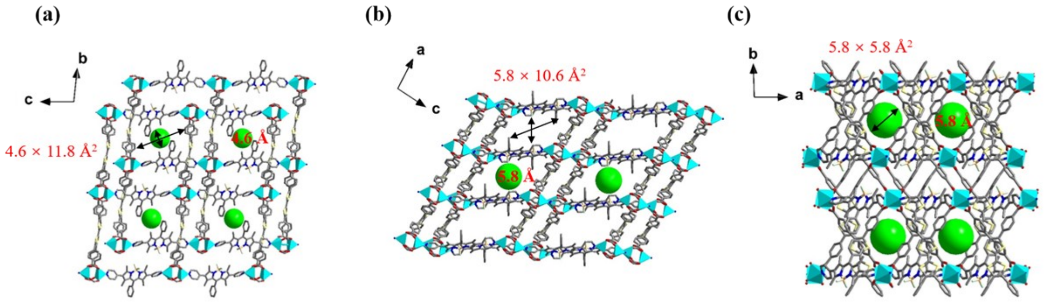

Fig. S2. Presentation of the 3D architecture of compound **1** from (a) *a* axis, (b) *b* axis and (c) *c* axis. (Green balls represent open channels)

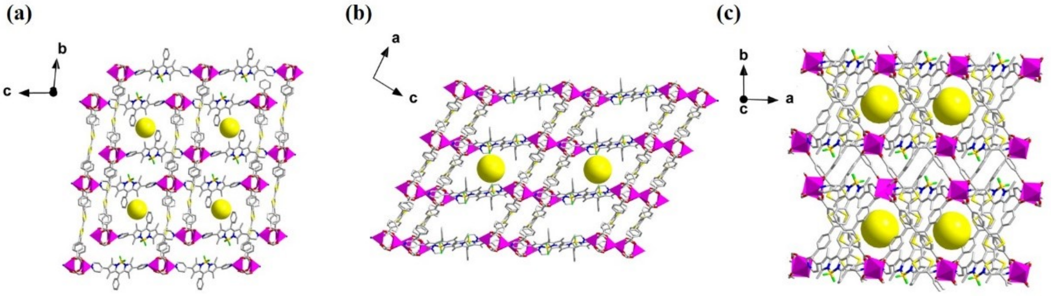

Fig. S3. Presentation of the 3D architecture of compound **2** from (a) *a* axis, (b) *b* axis and (c) *c* axis. (Yellow balls represent open channels)

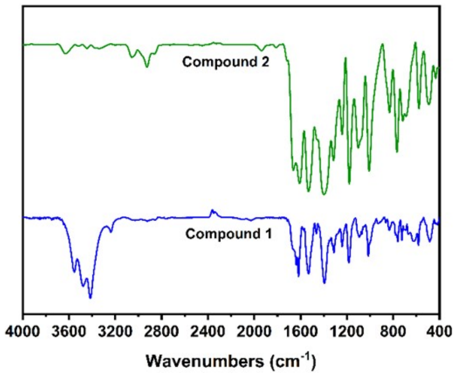

Fig. S4. The IR spectra of compounds **1** and **2**.

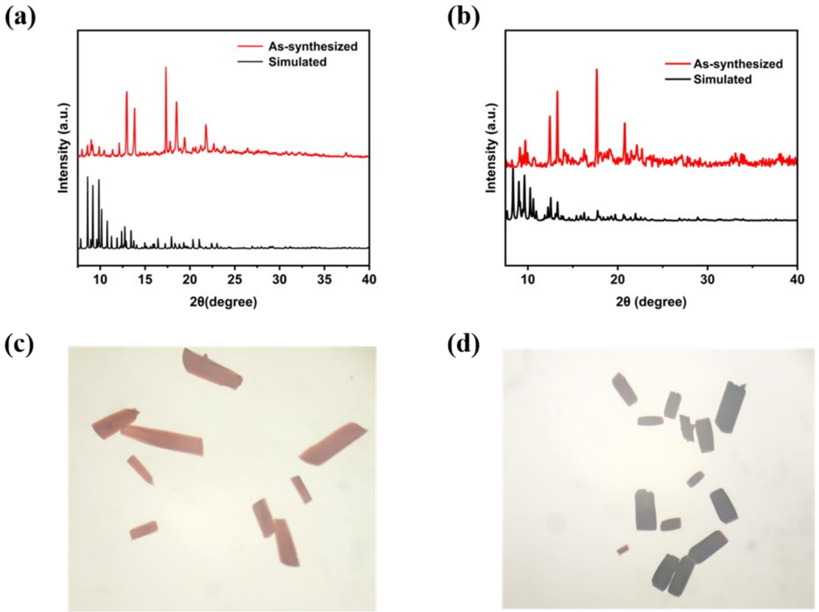

Fig. S5. PXRD patterns of reprepared (a) compound **1** and (b) compound **2**; Single crystal photos of compound **1** (c) and compound **2** (d).

Table S1. Crystallographic data and structure refinement for compounds 1 and 2.

	Compound **1**	Compound **2**
Formula	$C_{63}H_{41}BF_2N_4O_8S_4Zn_2$	$C_{63}H_{41}BCo_2F_2N_4O_8S_4$
Formula weight	1289.79	1276.91
Crystal system	triclinic	triclinic
Space group	*P*-1	*P*-1
a /Å	11.3593(7)	11.6011(10)
b /Å	19.4355(11)	19.3737(18)
c /Å	19.9874(13)	20.1834(18)
α /°	95.969(2)	93.837(5)
γ /°	95.883(2)	97.640(5)
β /°	91.084(2)	90.183(5)
V /Å^3	4363.7(5)	4485.7(7)
Z	2	2
ρ_{calcd}/g cm^{-3}	0.982	0.945
μ/mm^{-1}	1.275	0.506
Collected reflections	67011	49517
Unique reflections	20378	14465
R_1 $[I>2\sigma(I)]$	0.0588	0.0944
wR_2 (all data)	0.1670	0.2784
GOOF	1.084	1.027
CCDC	2296424	2323638

Table S2. Selected Bond Distances (Å) and Angles (deg) for compound 1.

Zn1−O5#2	2.0407(19)	Zn1−O5#2	2.0407(19)
Zn1−O7#5	2.050(2)	Zn2−O8#2	2.0590(19)
Zn1−O3#6	2.105(2)	Zn2−O6#3	2.0323(18)
Zn1−O1	2.022(2)	Zn2−O4	2.0222(19)
Zn1−N4	2.033(2)	Zn2−O2#1	2.087(2)
N1#4−Zn2−O2#2	98.94(9)	O8#1−Zn2−Zn1#2	84.36(5)
O5#1−Zn1−Zn2#5	83.55(5)	O8#1−Zn2−O2#2	151.96(8)
O5#1−Zn1−O7#6	86.47(8)	O6#3−Zn2−Zn1#2	74.01(5)
O5#1−Zn1−O3#5	150.27(8)	O6#3−Zn2−O8#1	85.19(8)
O7#6−Zn1−Zn2#5	73.70(5)	O6#3−Zn2−O2#2	86.80(8)
O7#6−Zn1−O3#5	86.16(8)	O4−Zn2−Zn1#2	91.15(6)
O3#5−Zn1−Zn2#5	66.74(6)	O4−Zn2−O8#1	92.76(8)
O1−Zn1−Zn2#5	89.97(6)	O4−Zn2−O6#3	165.15(8)
O1−Zn1−O5#1	93.05(8)	O4−Zn2−O2#2	88.20(8)
O1−Zn1−O7#6	163.62(8)	O4−Zn2−N1#4	97.67(9)
O1−Zn1−O3#5	86.20(9)	O2#2−Zn2−Zn1#2	67.60(6)
O1−Zn1−N4	99.02(9)	N1#4−Zn2−Zn1#2	163.75(7)
N4−Zn1−Zn2#5	156.03(7)	N1#4−Zn2−O8#1	108.68(9)
N4−Zn1−O5#1	117.80(9)	N1#4−Zn2−O6#3	96.92(8)
N4−Zn1−O7#6	95.65(9)	N4−Zn1−O3#5	91.59(9)

#1 +*x*, -1+*y*, +*z*; #2 1+*x*, +*y*, +*z*; #3 1+*x*, -1+*y*, +*z*; #4 2+*x*, +*y*, 1+*z*; #5 -1+*x*, +*y*, +*z*; #6 -1+*x*, -1+*y*, +*z*

Table S3. Selected Bond Distances (Å) and Angles (deg) for compound 2.

Co1-O3#3	2.082(5)	Co2-O7#4	2.060(4)
Co1-O8#2	2.031(4)	Co2-O6	2.023(5)
Co1-O5#1	2.055(5)	Co2-O2#5	2.078(5)
Co1-O1	1.987(5)	Co2-O4#6	2.013(5)
Co1-N4	2.073(5)	Co2-N1#7	2.052(5)
O3#3-Co1-Co2#2	70.94(15)	N1#6-Co2-O2#5	89.8(2)
O8#1-Co1-Co2#2	88.56(13)	O7#4-Co2-Co1#5	75.00(13)
O8#1-Co1-O5#2	85.53(19)	O7#4-Co2-O2#5	84.53(19)
O8#1-Co1-N4	106.2(2)	O6-Co2-Co1#5	88.37(14)
O8#1-Co1-O3#3	159.3(2)	O6-Co2-O7#4	87.48(19)
O5#2-Co1-Co2#2	75.19(13)	O6-Co2-O2#5	156.46(19)
O5#2-Co1-N4	92.1(2)	O6-Co2-N1#6	112.6(2)
O5#2-Co1-O3#3	86.3(2)	O2#5-Co2-Co1#5	68.18(13)
O1-Co1-Co2#2	93.62(14)	O4#7-Co2-Co1#5	91.46(15)
O1-Co1-O8#1	95.3(2)	O4#7-Co2-O7#4	166.1(2)
O1-Co1-O5#2	168.77(19)	O4#7-Co2-O6	95.2(2)
O1-Co1-N4	98.4(2)	O4#7-Co2-O2#5	87.7(2)
O1-Co1-O3#3	89.1(2)	O4#7-Co2-N1#6	99.4(2)
N4-Co1-Co2#2	159.87(17)	N1#6-Co2-Co1#5	155.08(17)
N4-Co1-O3#3	93.1(2)	N1#6-Co2-O7#4	92.04(19)

#1 +*x*, 1+*y*, +*z*; #2 -1+*x*, 1+*y*, +*z*; #3 -1+*x*, +*y*, +*z*; #4 1+*x*, +*y*, +*z*; #5 1+*x*, -1+*y*, +*z*; #6 2+*x*, -1+*y*, 1+*z*; #7 +*x*, -1+*y*, +*z*; #8 -2+*x*, 1+*y*, -1+*z*

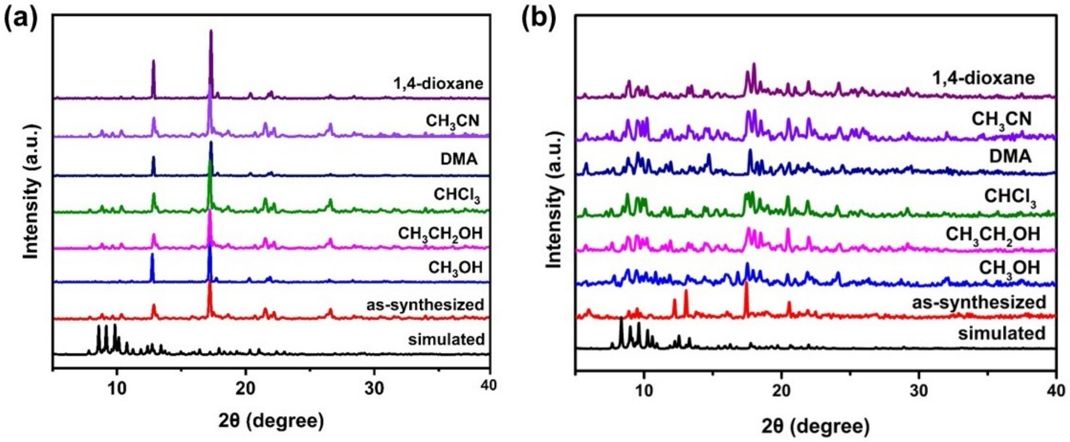

Fig. S6. PXRD patterns of compounds **1** and **2** in organic solvents for 24 hours.

Table S4. Solvent influence on the photoreductive dehalogenation reaction of 2-bromoacetophenone over compound 1.[a]

Entry	Solvent	Time [min]	Con.[%][b]
1	CH_3CN	30	3
2	CH_3OH	30	4
3	CH_3CH_2OH	30	4
4	CH_3Cl	30	97
5	DMSO	30	96
6	DMA	30	97
7	DMF	30	99

[a] Reaction conditions: Catalyst (3.0 mg), 2-bromoacetophenone (0.2 mmol), Hantzsch ester (0.22 mmol), DIPEA (40 μL), solvent (2.0 mL), 6 W white LED, air, 25.0 °C. [b]Determined by GC using dodecane as the internal standard.

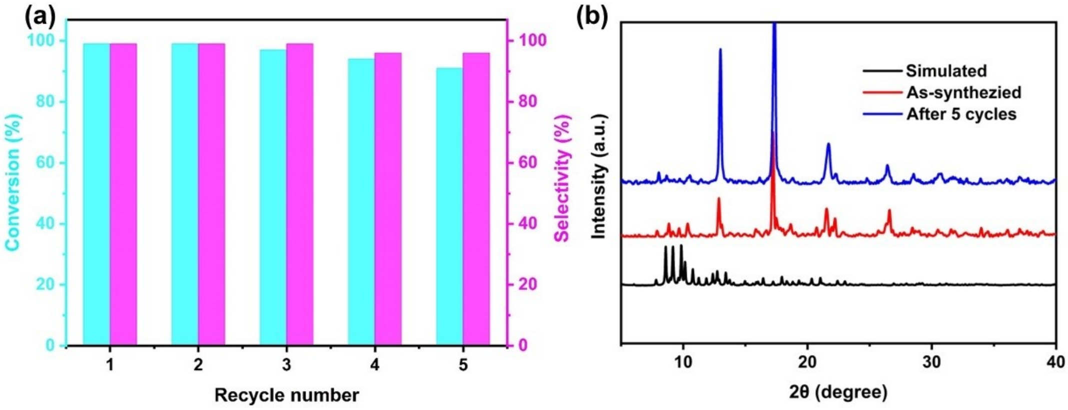

Fig. S7. (a) The reusability of compound **1** for photocatalytic dehalogenation reaction of 2-bromoacetophenone; (b) PXRD patterns for the simulated **1** and experimental **1** before and after the catalytic reaction.

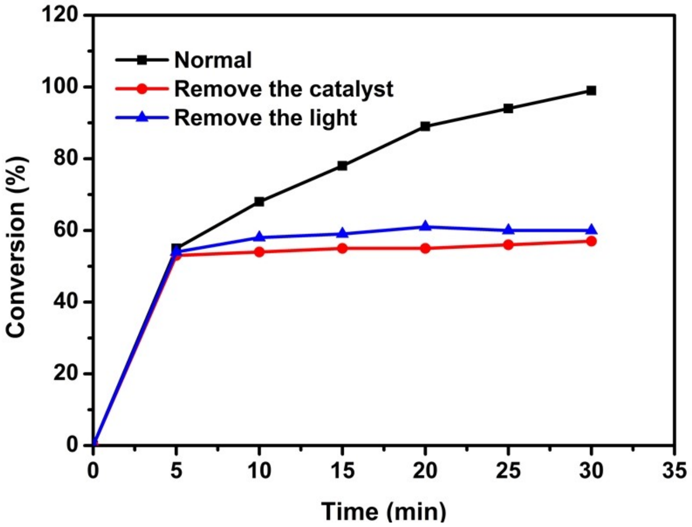

Fig. S8. (a) The time-conversion curve of photoreductive dehalogenation reaction of 2-bromoacetophenone over compound **1** under optimized reaction conditions. After 30 min of the reaction, the catalyst and light source were removed whereas the filtrate was further reacted under identical conditions: (black line) the common catalytic process, (red line) hot filtration test and (blue line) light source removal test.

Table S5. Performances of Photoreductive dehalogenation reaction of 2-bromoacetophenone using various photocatalysts.

Catalyst	Light source	Catalyst weight (mg)	Substrate amount (mmol)	Time (h)	Yield.(%)	TOF (mmol $g^{-1}h^{-1}$)	Reference
Eosin Y	A blue high-power LED (455 nm)	3.5	0.2	18	100	3.17	4
OH-TFP-TTA	30 W green LED (530 nm)	10	0.4	18	90	2.00	5
TiO$_2$	30 W green LED (530 nm)	10	0.4	18	19	0.42	5
CdS	30 W green LED (530 nm)	10	0.4	18	63	1.40	5
Hantzsch esters	14w CFLlamp	0.5mmol	0.1	4	97	0.19 h^{-1}	6
COF-JLU22	White LED	3	0.2	8	74	6.17	7
B-BT/glass fiber	White LED (> 420 nm)	6.4	-	-	-	80	8
Cz-POF-1	14 W compact Fluorescent lamp	5.0 µmol	0.2	24	98	1.63 h^{-1}	9
B$_2$-FL$_2$-BBT	23 W house hold light	10	0.2	4	93	4.65	10
PTBC-por COF	150 W Xe lamp (λ = 400–780 nm)	5	0.2	2	82	16.4	11
Compound 1	**6 W White LED**	**3**	**0.2**	**0.5**	**99**	**133.33 (172 h^{-1})**	**This work**
Compound 2	**6 W White LED**	**3**	**0.2**	**1**	**99**	**66.67 (85.13 h^{-1})**	**This work**

^{a}TOF = mmol product/(mmol catalyst×reaction time).

^{a}TOF = mmol product/(g catalyst×reaction time).

Table S6. Solvent influence on the photocatalytic aerobic oxidation of thiols over compound 2.[a]

Entry	Solvent	Time (min)	Con.[%][a]
1	CH_3CN	20	17
2	CH_3OH	20	28
3	CH_3CH_2OH	20	30
4	CH_3Cl	20	1
5	DMSO	20	17
6	1,4-dioxane	20	5
7	DMA	20	92
8	DMF	20	99

Reaction conditions: Catalyst (3.0 mg), substrate (0.1 mmol), solvent (1.0 mL), 6 W bule LED, air, 25.0 °C. [a]Determined by GC using 1,3,5-trimethoxybenzene as the internal standard.

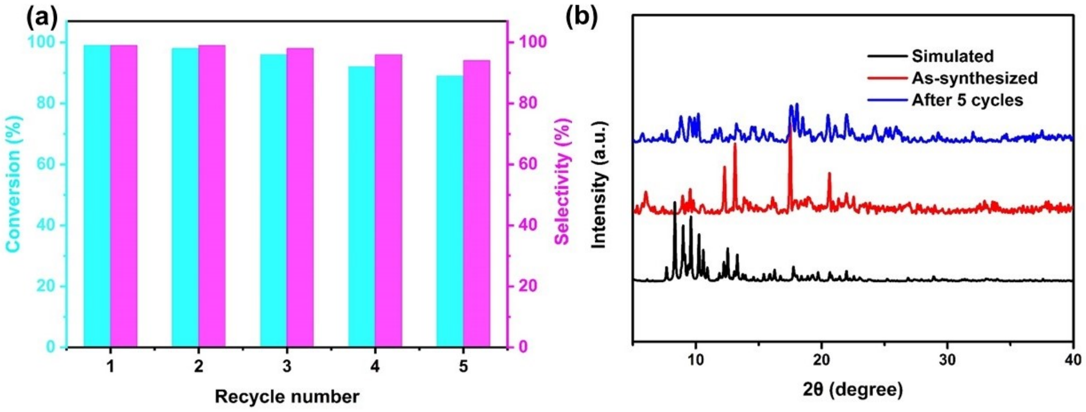

Fig. S9. (a) The reusability of compound **2** for photocatalytic oxidation of thiols; (b) PXRD patterns for the simulated **2** and experimental **2** before and after the catalytic reaction.

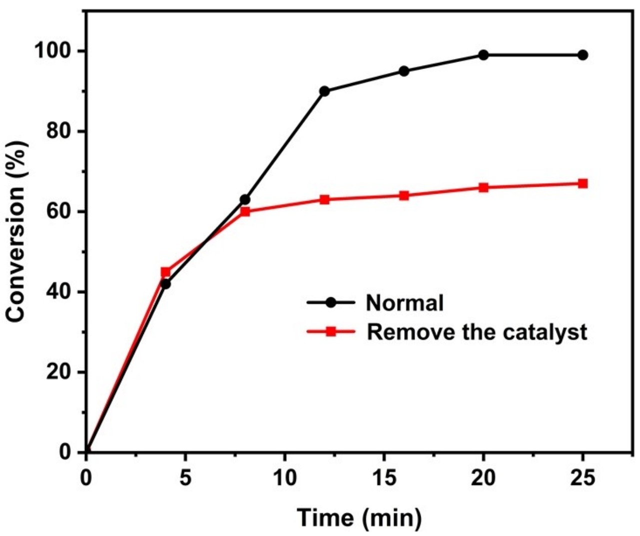

Fig. S10. The time-conversion curve of photocatalytic oxidation of thiols over compound **2.**

Table S7. Experimental results of the photocatalytic aerobic oxidation of thiophenols with Compound 2 as the catalyst[a]

Entry	Substrate	Product	Time [min]	Con. [%][b]	Sel. [%][b]
1	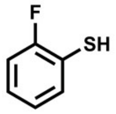	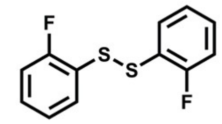	40	99	98
2	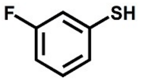	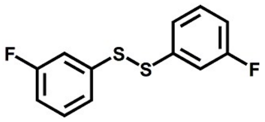	20	99	98
3	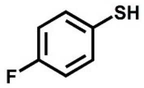	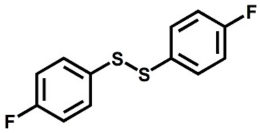	25	99	97
4	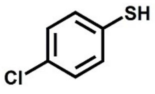	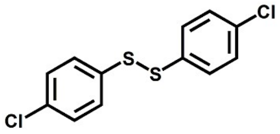	15	99	86
5	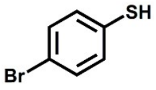	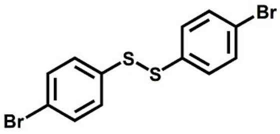	20	99	97
6	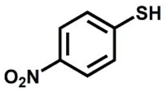	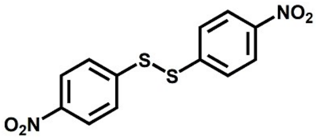	20	99	96
7	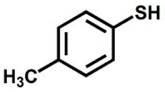	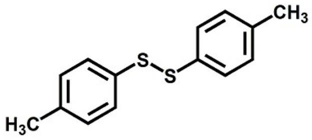	25	99	99
8	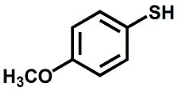	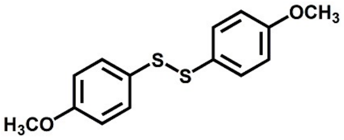	25	99	99
9	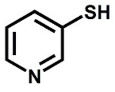	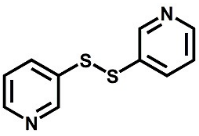	15	99	96

[a] Reaction conditions: Catalyst (3.0 mg), substrate (0.1 mmol), 1 mL DMF, 6 W bule LED, air,

25.0 °C. [b] Determined by GC using 1,3,5-trimethoxybenzene as the internal standard.

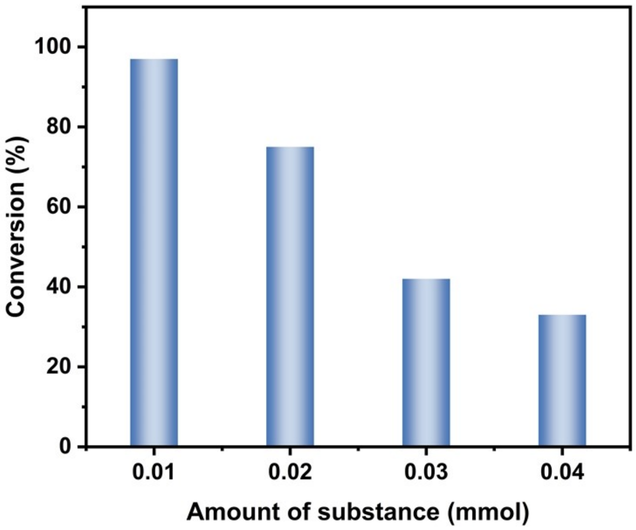

Fig. S11. Concentration influence of BQ for $O_2^{\bullet-}$ on thiols oxidative over compound **2.**

Table S8. Performances of photocatalytic aerobic oxidation of thiols using various photocatalysts.

Catalyst	Light source	Catalyst [mg]	Substrate [mmol]	Time [h]	Conv. [%]	TOF [mmol g^{-1} h^{-1}][a]	Reference
$CsPbBr_3$	white LEDs (9 W)	1 mmol%	0.2	6	98	3h^{-1}	12
CdSe QDs	high-pressure mercury lamp (500 W)	0.02 mmol	0.5	4	99	6.25 h^{-1}	13
Phenylglyoxylic acid	30 W green LED (530 nm)	1 mmol%	0.5	7	99	7 h^{-1}	14
$PtS/ZnIn_2S_4$	Visible light	5	0.1	6	99	3.33	15
MFC-CMP	Bule LED	5	0.6	0.5	91	240	16
TiO_2	Green LED (520 nm)	30	0.6	0.67	91	29.8	17
OBCP	LED irradiation (460 nm)	-	0.1	12	99	-	18
CdSe/CdS NRs	Blue LED light (415 nm)	0.15 mol%	0.2	6	87	22 h^{-1}	19
Ln-CPs	visible light	7.4	0.2	8	99	3.38	20
Compound 2	**6 W Bule LED (450-465 nm)**	**3**	**0.1**	**0.33**	**99**	**101 (130 h^{-1})**	**This work**
Compound 1	**6 W Bule LED (450-465 nm)**	**3**	**0.1**	**1**	**99**	**33.3 (42.57 h^{-1})**	**This work**

[a] TOF = mmol product/(mmol catalyst×reaction time).

[a] TOF = mmol product/(g catalyst×reaction time).

References

(1) G.M. Sheldrick, A Short History of SHELX, *Acta Cryst.*, 2008, **A64**, 112–122.

(2) G. M. Sheldrick, Crystal Structure Refinement with SHELXL, *Acta Cryst.*, 2015, **C71**, 3–8.

(3) H. Krupitsky, Z. Stein, I. Goldberg and C. E. Strouse, Crystalline Complexes, Coordination Polymers and Aggregation Modes of Tetra(4-pyridyl)porphyrin, *J. lncl. Phenom. Mol. Recogn. Chem.*, 1994, **18**, 177–192.

(4) M. Neumann, S. Füldner, B. König and K. Zeitler, Metal-Free, Cooperative Asymmetric Organophotoredox Catalysis with Visible Light, *Angew. Chem. Int. Edn.*, 2011, **50**, 951–954.

(5) H. R. Liu, C. Z. Li, H. Li, Y. Q. Ren, J. Chen, J. T. Tang and Q. H. Yang, Structural Engineering of Two-Dimensional Covalent Organic Frameworks for Visible-Light-Driven Organic Transformations, *ACS Appl. Mater. Interfaces*, 2020, **12**, 20354–20365.

(6) J. Jung, J. Kim, G. Park, Y. M. You and E. J. Cho, Selective Debromination and α-Hydroxylation of α-Bromo Ketones Using Hantzsch Esters as Photoreductants, *Adv. Synth. Catal.*, 2016, **358**, 74–80.

(7) Z. P. Li, Y. F. Zhi, P. P. Shao, H. Xia, G. S. Li, X. Feng, X. Chen, Z. Shi and X. M. Liu, Covalent Organic Framework as an Efficient, Metal-Free, Heterogeneous Photocatalyst for Organic Transformations under Visible Light, *Appl. Catal. B: Environ.*, 2019, **245**, 334–342.

(8) W. Huang, B. C. Y. Ma, D. Wang, Z. J. Wang, R. Li, L. Wang, K. Landfester and K. A. I. Zhang, A Fixed-Bed Photoreactor using Conjugated Nanoporous Polymer-Coated Glass Fibers for Visible Light-Promoted Continuous Photoredox Reactions, *J. Mater. Chem. A*, 2017, **5**, 3792–3797.

(9) J. Luo, X. Zhang and J. Zhang, Carbazolic Porous Organic Framework as an Efficient, Metal-Free Visible-Light Photocatalyst for Organic Synthesis, *ACS Catal.*, 2015, **5**, 2250−2254.

(10) Z. J. Wang, S. Ghasimi, K. Landfestera and K. A. I. Zhang, A Conjugated Porous Poly-Benzobisthiadiazole Network for a Visible Light-Driven Photoredox Reaction, *J. Mater. Chem. A*, 2014, **2**, 18720.

(11) H. C. Shan, D. Ca, X. X. Zhang, Q. Zhu, P. Y. Qin, J. Baeyens, Donor-Acceptor Type Two-Dimensional Porphyrin-Based Covalent Organic Framework for Visible-

Light-Driven Heterogeneous Photocatalysis, *Chem. Eng. J.*, 2022, **432**, 134288.

(12) W. B. Wu, Y. C. Wong, Z. K. Tan and J. Wu, Photo-Induced Thiol Coupling and C–H Activation using Nanocrystalline Lead-Halide Perovskite Catalysts, *Catal. Sci. Technol.*, 2018, **8**, 4257.

(13) X. B. Li, Z. J. Li, Y. J. Gao, Q. Y. Meng, S. Yu, R. G. Weiss, C. H. Tung, L. Z. Wu, Mechanistic Insights into the Interface-Directed Transformation of Thiols into Disulfides and Molecular Hydrogen by Visible-Light Irradiation of Quantum Dots, *Angew. Chem. Int. Ed.*, 2014, **53**, 2085–2089.

(14) N. Spiliopouloua and C. G. Kokotos, Photochemical Metal-Free Aerobic Oxidation of Thiols to Disulfides, *Green Chem.*, 2021, **23**, 546.

(15) E. Grabowska, M. Diak, M. Marchelek and A. Zaleska, Photocatalytic Splitting of Thiols to Produce Disulfides and Hydrogen over PtS/$ZnIn_2S_4$ Nanocomposites under Visible Light, *Appl. Catal. B: Environ.*, 2018, **234**, 50–55.

(16) X. Y. Dong, H. M. Hao, F. L. Zhang and X. J. Lang, Combining Brønsted Base and Photocatalysis into Conjugated Microporous Polymers: Visible Light-Induced Oxidation of Thiols into Disulfides with Oxygen, *J. Colloid Interf. Sci.*, 2022, **622**, 1045–1053.

(17) H. Xu, J. L. Shi, Sh. Sh. Lyu and X. J. Lang, Visible-Light Photocatalytic Selective Aerobic Oxidation of Thiols to Disulfides on Anatase TiO_2, *Chinese Journal of Catalysis*., 2020, **41**, 1468–1473.

(18) X. Y. Huang, Y. L. Lu, G. J. Mao, Sh. H. Yin, B. Long, G. J. Deng, A. Alid and T. Song, Polarization Engineering of Porous Organic Polymers for Superior Photocatalytic Synthesis of Disulfides and CO_2 Reduction, *J. Mater. Chem. A*, 2022, **10**, 24147–24155.

(19) Y. C. Sha, X. M. Lin, J. Niklas, O. Poluektov, B. Diroll, Y. L. Lin, J. G. Wen, Z. Hood, A. W. Lei and E. Shevchenko, Insights into the Extraction of Photogenerated Holes from CdSe/CdS Nanorods for Oxidative Organic Catalysis, *J. Mater. Chem. A*, 2021, **9**, 12690–12699.

(20) S. Y. An, Z. F. Guo, X. Liu, Y. Che, H. Z. Xing and P. Chen, Visible-Light-Responsive Lanthanide Coordination Polymers for Highly Efficient Photocatalytic Aerobic Oxidation of Amines and Thiols, *New J. Chem.*, 2021, **45**, 15767–15775.